

Title	Mid-infrared optical sensing using sub-wavelength gratings
Authors	Hogan, Brian;Lewis, Liam;McAuliffe, Michael;Hegarty, Stephen P.
Publication date	2019-02-04
Original Citation	Hogan, B., Lewis, L., McAuliffe, M. and Hegarty, S.P., 2019. Mid-infrared optical sensing using sub-wavelength gratings. Optics express, 27(3), (10pp). DOI:10.1364/OE.27.003169
Type of publication	Article (peer-reviewed)
Link to publisher's version	https://www.osapublishing.org/oe/abstract.cfm?uri=oe-27-3-3169 - 10.1364/OE.27.003169
Rights	© 2019 Optical Society of America under the terms of the OSA Open Access Publishing Agreement - https://creativecommons.org/licenses/by/4.0/
Download date	2025-07-07 20:02:09
Item downloaded from	https://hdl.handle.net/10468/9150



UCC

University College Cork, Ireland
 Coláiste na hOllscoile Corcaigh



Mid-infrared optical sensing using sub-wavelength gratings

BRIAN HOGAN,^{1,2,*} LIAM LEWIS,^{1,2} MICHAEL MCAULIFFE,¹ AND STEPHEN P. HEGARTY^{1,2}

¹Centre for Advanced Photonics and Process Analysis, Cork Institute of Technology, Cork, Ireland

²Tyndall National Institute, University College Cork, Cork, Ireland

*brian.hogan@mycit.ie

Abstract: Optical sensing has shown great potential for both quantitative and qualitative analysis of compounds. In particular sensors which are capable of detecting changes in refractive index at a surface as well as in bulk material have received much attention. Much of the recent research has focused on developing technologies that enable such sensors to be deployed in an integrated photonic device. In this work we demonstrate experimentally, using a sub-wavelength grating the detection of ethanol in aqueous solution by interrogating its large absorption band at $9.54\ \mu\text{m}$. Theoretical investigation of the operating principle of our grating sensor shows that in general, as the total field interacting with the analyte is increased, the corresponding absorption is also increased. We also theoretically demonstrate how sub-wavelength gratings can detect changes in the real part of the refractive index, similar to conventional refractive index (RI) sensors.

© 2019 Optical Society of America under the terms of the [OSA Open Access Publishing Agreement](#)

1. Introduction

Recently there has been much research interest in optical sensing technologies. Such technologies measure changes in the optical properties of the light in a sensing system following interaction with an analyte. There is also much commercial interest in the development of these technologies for applications such as bio-sensing, food and beverage, pharmaceutical, air & water quality, security and mining.

In particular, refractive index (RI) sensors have attracted much attention. When designed and configured appropriately these devices exhibit resonant features such as reflection peaks or dips which are affected by the RI of the analyte material. While devices such as the Surface Plasmon Resonance (SPR) sensor [1–3] have become a popular choice for many sensing applications, there has been considerable interest in sensors such as the Bloch Surface Wave (BSW) sensor [4–6], micro-ring resonator sensor [7, 8] and the Mach-Zender Interferometer (MZI) sensor [9, 10]. Furthermore, these devices have been realised based on silicon structures and as such can be deployed in integrated photonic devices.

While Sub-Wavelength Gratings (SWG) have been the focus of research for some time [11, 12] they have attracted much attention lately because of their interesting and useful properties. With the appropriate design and fabrication these devices can be used as broadband reflectors [13, 14] or also as optical filters with ultra high Q-factors [14, 15]. In [16, 17], focusing mirrors and lenses were developed using this grating structure by spatially controlling the phase of the reflection. In recent work [18] we have shown how SWGs can be deployed at longer wavelengths around $10\ \mu\text{m}$ using suitable materials. We have also shown that the Zero Contrast Grating (ZCG) structure can be slightly modified to allow for more robust fabrication, without significant penalty in terms of grating performance [19].

At present the standard technology for sensing applications where the absorption band of a given material is to be interrogated is the Attenuated Total Reflector (ATR) [20, 21]. This technology works by coupling light at an angle into a high refractive index bulk medium on which sits a lower index analyte material such that total internal reflection occurs.

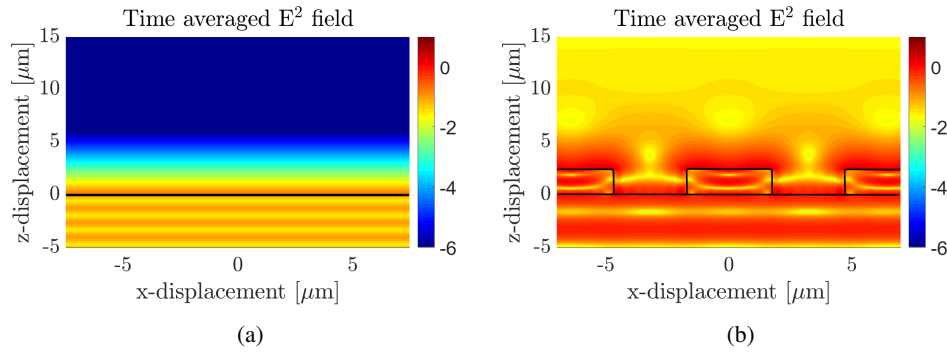


Fig. 1. (a) Log_{10} of time averaged E^2 field in ATR device, $\theta_i = 25^\circ$, TM polarisation. (b) Log_{10} of time averaged E^2 field in HCG, normally incident TM polarised light. Field values are calculated at $9.54 \mu\text{m}$ using Rigorous Coupled Wave Analysis (RCWA).

As shown by Harrick [22] an exponentially decaying evanescent field extends into the analyte material. When the analyte material which sits atop the ATR is lossy the overlap between this analyte and the evanescent field results in the internally reflected light becoming frustrated. This manifests as a drop in the reflectivity from the device throughout the material absorption band.

A notable feature of SWGs is the high field strengths that are established around the grating bars in the low index region. Fig. 1(a) shows the time averaged E^2 field for a germanium ATR under TM polarised incidence at 25° . Figure 1(b) shows the time averaged E^2 field for a HCG under normally incident TM polarised light. It should be noted that for the grating structure a larger field resides in the analyte. For illustrative purposes the log_{10} of the field was plotted to allow for a clear visual interpretation of the difference in the field interacting with the analyte.

From this plot it is clear that the SWG allows for a greater overlap between field and analyte and accordingly a larger sensitivity to absorption is expected when compared to an ATR. This highlights the promise of such grating structures for absorption based sensing. Absorption based sensing is of particular interest at wavelengths around $10 \mu\text{m}$ where many materials have vibrational fingerprints. In this work we demonstrate how SWGs can act as a probe in an optical sensing system and we experimentally use our modified ES-ZCG device [19] to interrogate the absorption bands of ethanol at wavelengths from $8 \mu\text{m}$ - $10 \mu\text{m}$.

2. Simulations and grating sensor design

The Etch Stop ZCG (ES-ZCG) as reported in [19] is shown in Fig. 2(a). In this structure an etch-stop layer of thickness (d_e) is sandwiched between the two high index layers, one of which is a periodically spaced grating layer. The duty-cycle (DC) is defined as the ratio of the grating bar width (w) to the period (Λ) ($\text{DC} = w / \Lambda$). Additionally in Fig. 2(b) we show a schematic diagram of a HCG with high index bars of thickness t_g on top of a low index substrate. For the grating sensor it is proposed that light incident from beneath the substrate will interact with analyte residing between and above the grating bars and the resulting reflectivity will be altered depending on the composition of the analyte solution.

Rigorous Coupled Wave Analysis (RCWA) [23–26] was used to numerically calculate grating performance. Our grating materials, Germanium (Ge) and Strontium Fluoride (SrF_2) are shown to have negligible dispersion and loss in our wavelength range [27–30] and for ease of simulation were assumed to be lossless and non-dispersive. The wavelength dependant loss and dispersion values for our water and ethanol analyte materials [31,32] were included in simulations.

In this work two types of responses are investigated. Frustrated reflection resulting from the

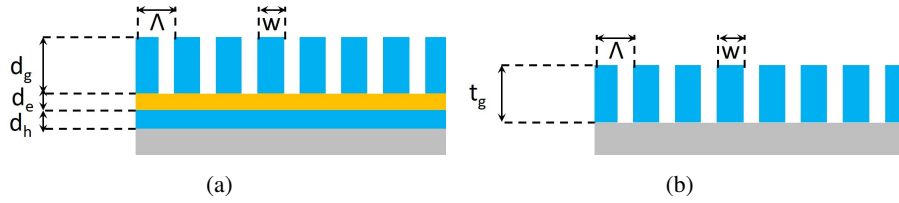


Fig. 2. (a) Schematic diagram of ES-ZCG structure. (b) Schematic diagram of HCG structure.

interaction between the evanescent field and the analyte will first be investigated. In addition, a shift in the central wavelength of a narrow reflection feature which results from a change in the real part of the index of the analyte will be investigated. These effects will be demonstrated through numerical simulation and verified through experimental measurement.

Ethanol has been shown to have a large absorption peak at $9.54 \mu\text{m}$ [32]. Ideally an absorption based grating sensor should be designed such that it has maximum sensitivity to changes in extinction coefficient (k) at the wavelength for which k is a maximum. In order to identify a grating with optimum parameters, an extensive parameter scan was conducted. This scanning procedure was expedited by only considering HCGs as they have fewer geometric parameters than the ES-ZCG. Reflectivity values were calculated for water and different ethanol concentrations in the superstrate (between and above the grating bars).

Each reflectivity measurement of an analyte (R_{analyte}) solution was normalised against the reflectivity for pure water (R_{water}). This normalised reflectivity (NR) value was calculated as shown in Eq. (1).

$$NR = \frac{R_{\text{analyte}}}{R_{\text{water}}} \quad (1)$$

The grating parameter set yielding the largest drop in normalised reflectivity ($\Delta NR = 1 - NR$) was taken as an optimum grating parameter set. Consideration should also be given to the raw reflectivity of the grating. When the grating reflectivity values are low it was possible to obtain large changes in normalised reflectivity for small changes in absolute reflectivity. While theoretically this should improve sensitivity it may not be possible to measure such small changes in reflectivity and the resolution of the device may be compromised. To mitigate this, only the grating parameter sets which have a minimum raw reflectivity value of 40% for water solutions at $9.54 \mu\text{m}$ were considered.

2.1. TM polarised grating sensor simulation

A sensitive design identified in the scan for TM polarised light was, $\Lambda = 6450 \text{ nm}$, $DC = 0.54$, $t_g = 2415 \text{ nm}$ is shown in Fig. 3(a). In terms of fabrication tolerance, a $\pm 100 \text{ nm}$ error in barwidth and a $\pm 50 \text{ nm}$ error in grating thickness did not cause significant penalty to sensor performance in terms of ΔNR , nor did a $\pm 7^\circ$ incident angle.

For this optimised HCG, when the superstrate comprises a 20% ethanol solution the normalised reflectivity from the grating was 0.4411, a relative reflectivity drop of almost 56%. Furthermore, as demonstrated by comparing Fig. 3(a) and Fig. 3(c) the response from this single reflection HCG sensor is comparable to an ATR with $\theta_i = 25^\circ$ and 5 internal reflections.

Figures 3(b) and 3(d) show the raw reflectivities of the HCG and ATR respectively. Furthermore comparison of Figs. 3(b) and 3(d) shows that the absolute reflectivity from the HCG is greater than that of the ATR. In terms of device performance this should allow for a superior Signal to

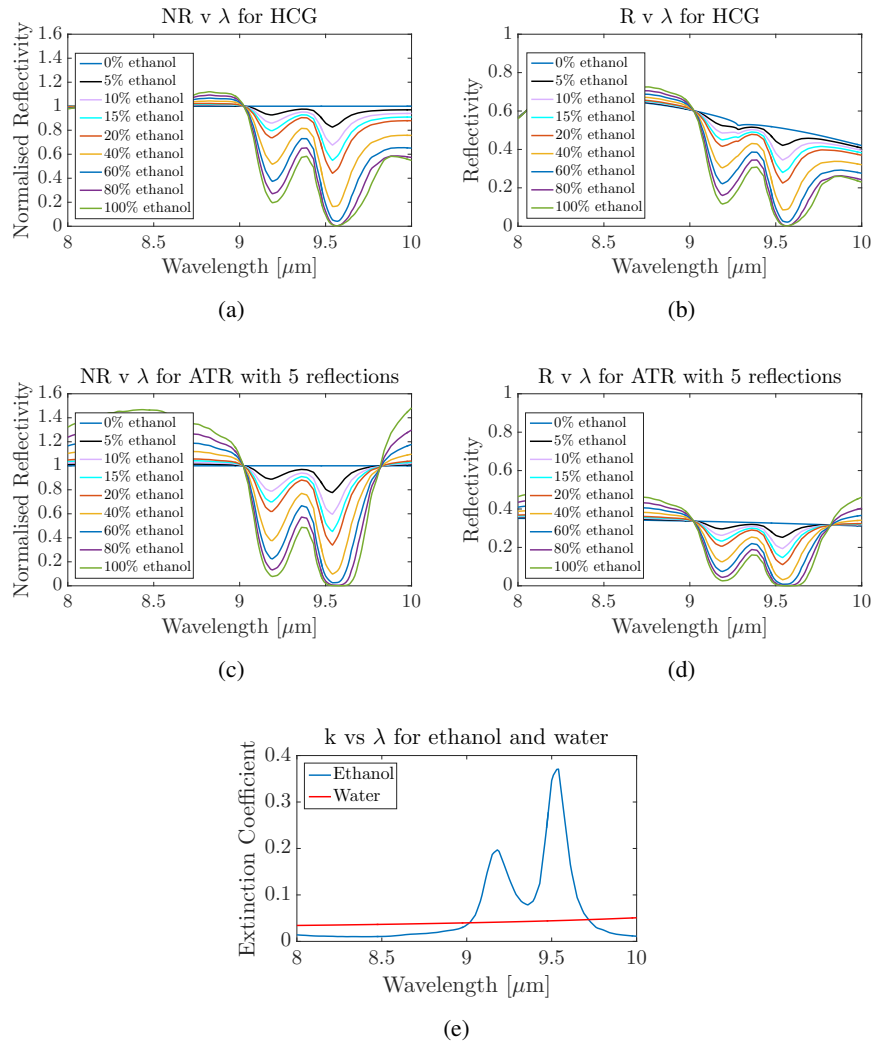


Fig. 3. (a) Normalised reflectivity spectra for TM polarised optimised HCG with ethanol concentration between 0 - 100%. (b) Reflectivity from optimised HCG with ethanol concentrations between 0 - 100%. (c) Normalised reflectivity spectra for a 5-reflection ATR with ethanol concentration between 0 - 20%. (d) Reflectivity for 5-reflection ATR with ethanol concentration between 0 - 100%. (e) Extinction coefficient (k) for ethanol and water as a function of wavelength.

Noise Ratio (SNR) when incorporated into a full sensing system.

In comparing Figs. 1(a) and 1(b) it is clear that in the case of the grating structure there is a greater overlap between the field and the analyte compared to the ATR structure. For a number of different grating geometries the total time-averaged E^2 Field in one unit cell was computed and normalised to an input wave with the same unit cell. A sensitivity value ($\Delta NR/\Delta C$) describing the relative drop in normalised reflectivity (ΔNR) for a given change in ethanol concentration (ΔC) was also computed for each grating geometry. The resultant plot shown in Fig. 4 shows that for the most part, as the field residing in the analyte increases, so too does the sensitivity.

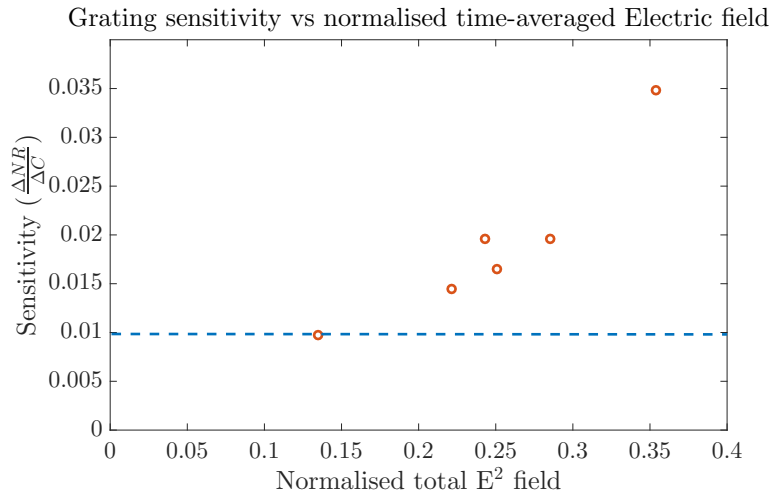


Fig. 4. Sensitivity vs total, normalised, time-averaged E^2 field for various grating geometries and a reference line showing sensitivity of an ATR with $\theta_i = 25^\circ$ at wavelength of $9.54 \mu\text{m}$.

The field values displayed in Fig. 4 comprise the total field belonging to both the transmitted and reflected modes for each grating geometry. While this approach does not reveal the precise nature of the relationship between device sensitivity and the amount of field interacting with analyte it does highlight the general trend which forms the basis of our experimental work.

While other literature has investigated the use of SWGs as refractive index sensors [33, 34] these works interrogate the real part of the refractive index. To the best of our knowledge, SWGs have not been proposed as a means of interrogating the imaginary part of the refractive index before. This work highlights the potential for SWGs to be deployed as sensing transducers in a very important spectral region as a viable alternative to the Attenuated Total Reflector (ATR).

2.2. TE polarised grating sensor simulation

In [35] the authors explain that the strong confinement of TE modes in the waveguide can be useful for refractive index sensing. In this section we numerically demonstrate that SWGs can be used as RI sensors. For an appropriately designed grating, a change in the real part of the analyte index can induce a wavelength shift in a narrow reflection or transmission feature. Furthermore we demonstrate the superior sensor performance that can be realised when this reflection or transmission feature shifts near or at a material's absorption band. Following a parameter scan, a grating with parameters ($\Lambda = 4463 \text{ nm}$, $\text{DC} = 56\%$, $t_g = 2723 \text{ nm}$) was identified as having a useful reflectivity response to ethanol in the superstrate for TE polarised input light.

Figure 5(a) shows the simulated reflectivity response for this grating. As with simulations shown in Fig. 3 the reflectivities for different ethanol concentrations are normalised with respect to the reflectivity for pure water in the superstrate. Fig. 5(a) shows that for a solution with 20% ethanol concentration the normalised reflectivity drops to 25.2%, a significant improvement over its absorption based counterpart.

To gain insight into this enhanced response it is useful to consider the un-normalised reflectivity profiles for the different solutions as shown in Fig. 5(b). While there is a drop in reflectivity at $9.54 \mu\text{m}$ due to the ethanol absorption there is also a shift in the reflection profile due to the change in real part of refractive index. Interestingly as the feature is shifted it moves to wavelengths where the absorption due to water is larger than absorption due to ethanol and the

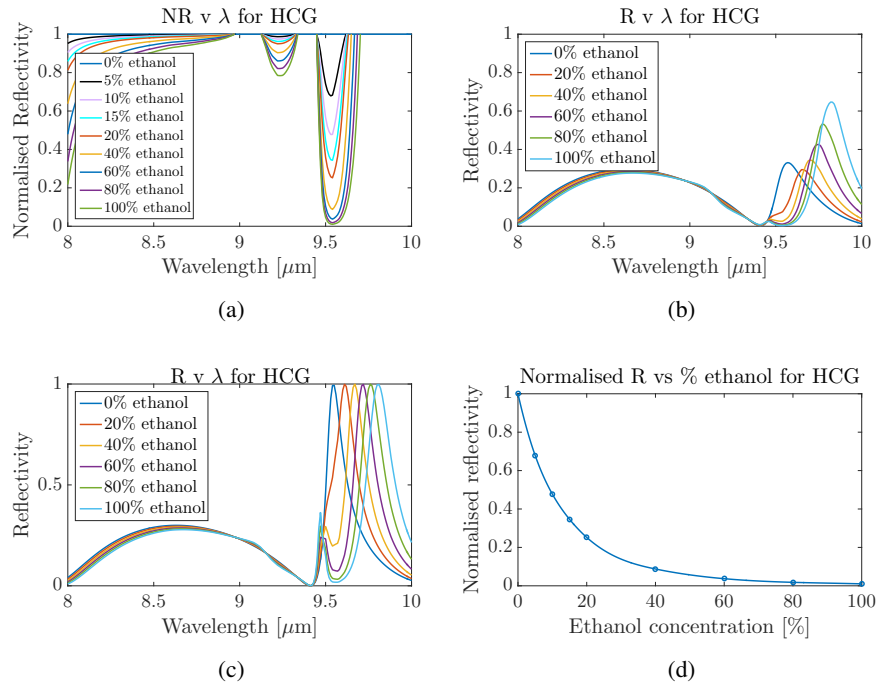


Fig. 5. (a) Normalised reflectivity spectra for TE polarised HCG with ethanol concentration between 0 - 100%. (b) Raw HCG reflectivity profiles for ethanol concentration between 0 - 100% under TE polarised incident light. (c) Raw HCG reflectivities where imaginary part of the refractive index remains constant for all ethanol concentrations. (d) Normalised reflectivity of TE polarised HCG as a function of ethanol concentration at 9.54 μm .

magnitude begins to increase for increasing ethanol concentration.

In order to confirm that the wavelength shift is being driven by the real part of the refractive index, a calculation was made where only the real part of the index was updated and the imaginary part was kept at 0. While this is not physically possible it does allow for a certain level of insight into the mechanism governing the shift in reflection profile. Figure 5(c) shows the raw reflectivity profiles of the grating sensor with $k=0$ for all analyte solutions. With only the real part of the refractive index changing from one ethanol concentration to the next, there is a clear shift in reflection peak.

By utilising the impact of both the real and imaginary components of the index on the reflected light, enhanced sensitivity can be obtained as shown in Fig. 5(a). The sensor, in this instance is quite sensitive to changes for small ethanol concentrations as shown in Fig. 5(d). While the limit of detection for a sensing system using SWGs will depend on the spectral & noise properties of the source and detector and thus the SNR of the system, the HCG described here can be shown to be most sensitive at lower concentrations. Normalised reflectivity as a function of ethanol concentration is shown in Fig. 5(d).

3. Experimental measurements

While the numerical simulations above describe optimised grating geometry performance, we used a previously fabricated ES-ZCG which had been designed and optimised as a reflector in

air [19]. While this grating was not designed with absorption or RI based sensing of ethanol in mind, a significant sensitivity for this grating was simulated. In this section we will show that our fabricated grating is capable of operation as both a RI sensor and an absorption based sensor.

Reflectance measurements were made using a commercially sourced Quantum Cascade Laser (QCL) with an operating wavelength range of between $6.1\ \mu\text{m}$ and $10.7\ \mu\text{m}$ (Block Engineering LaserTune QCL). A gold coated 90° knife-edge prism was used to guide light appropriately as shown in the schematic diagram in Fig. 6(a). In this setup the ES-ZCG was placed a distance from the prism such that the angle of incidence was approximately 1° . The analyte lay on the ES-ZCG surface as shown in the schematic.

The ES-ZCG used here had the following geometric properties ($\Lambda = 4000\ \text{nm}$, $\text{DC} = 56\%$, $d_g = 2295\ \text{nm}$, $d_h = 395\ \text{nm}$, $d_e = 95\ \text{nm}$). Reflectivity measurements were taken for ethanol concentration which increased in intervals of 20% . The reflectivity from the grating for each ethanol solution was normalised against the grating reflectivity for a pure water sample. These reflection measurements were made using both TM and TE polarised light. As with the gratings described in the simulation section, for TE polarised reflection our fabricated grating was affected by both the real and imaginary part of the analyte index. A direct measurement of the absorption band was realised through measurements with TM polarised light.

Figures 6(c) and 6(d) show the predicted and measured reflectivities for TM polarised input light. There is good agreement between numerically predicted and experimentally measured

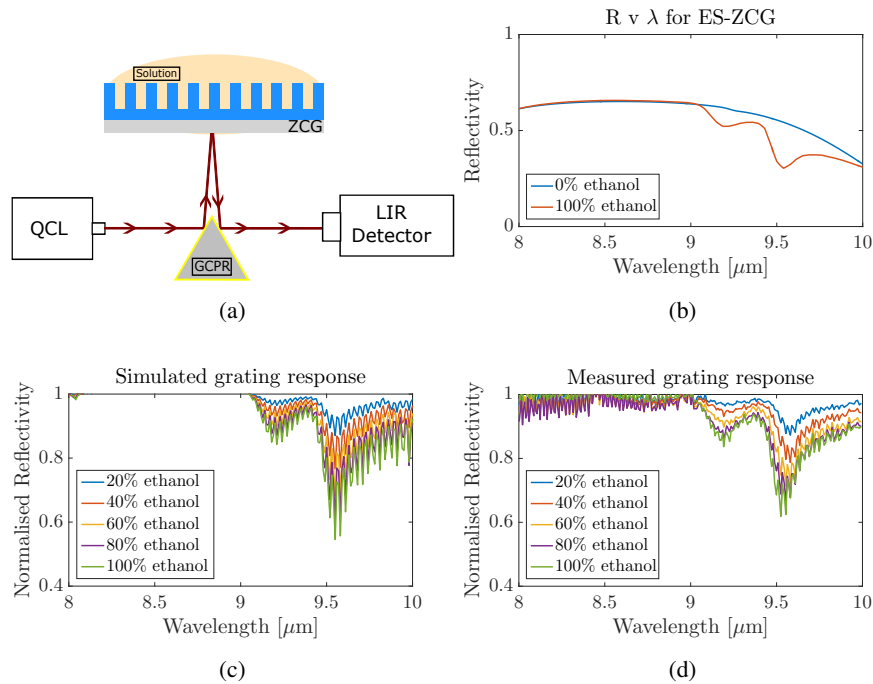


Fig. 6. (a) Schematic diagram of experimental setup. Quantum Cascade Laser (QCL), Gold-Coated Prism Reflector (GCPR), Longwave InfraRed (LIR) detector (MSL-12 HgCdTe commercially sourced from Infrared Associates). (b) Simulated reflectivities of measured grating for ethanol and water under TM polarised light. (c) Simulated normalised reflection spectrum for HCG with ethanol concentration between 0 - 100% for TM polarised light. (d) Measured NR spectrum for HCG with ethanol concentration between 0 - 100% for TM polarised light.

reflectivity values in terms of shape and magnitude of the overall response. The simulated raw reflectivity of this grating for both ethanol and water is shown in Fig. 6(b). As expected two clear reflection dips are visible for the ethanol absorption bands showing that this ES-ZCG sensor operates as an absorption sensor in TM polarisation.

Figures 7(a) and 7(b) show the predicted and measured reflectivities for TE polarised light. These Figs. also show good agreement between numerically predicted and experimentally values. For the TE polarised response the normalised reflectivity dip is not at $9.54\ \mu\text{m}$ where ethanol absorption occurs. Figure 7(c) shows the raw reflectivity curves for water and ethanol. There is a clear shift in the reflection dip to higher wavelengths as the ethanol concentration increases and this prompts the large dip in the normalised reflectivity at $9.68\ \mu\text{m}$ as shown in Fig. 7(b).

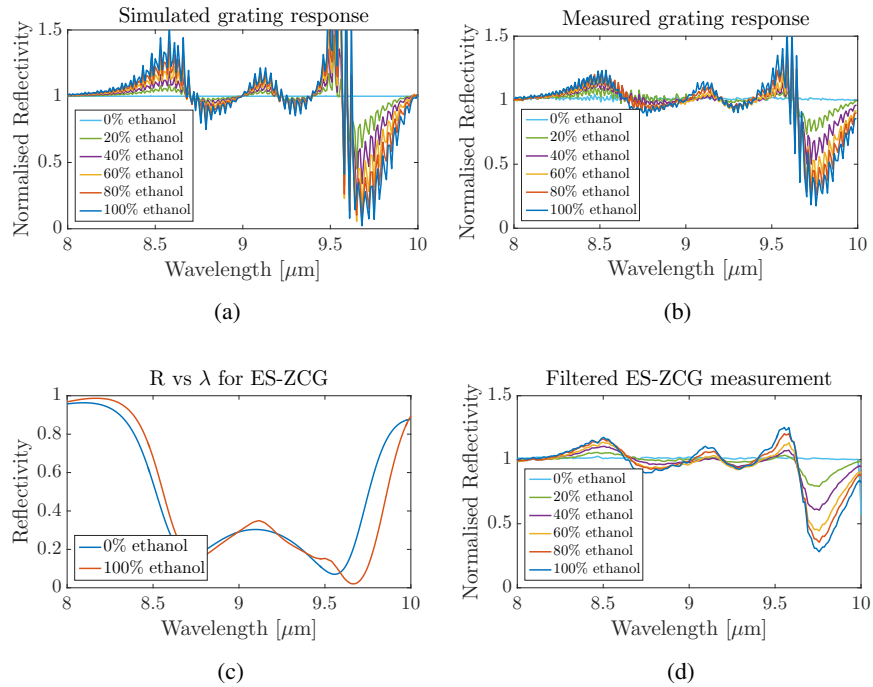


Fig. 7. (a) Simulated normalised reflection spectrum for ES-ZCG with ethanol concentration between 0 - 100% under TE polarised light. (b) Measured normalised reflection spectrum for ES-ZCG with ethanol concentration between 0 - 100% under TE polarised light. (c) Raw reflectivities of fabricated ES-ZCG for pure water and pure ethanol under TE polarised light. (d) Measured normalised reflectivity spectra after use of filtering algorithm in Unscramblr software.

As reported in [19] an interference pattern is observed in the grating reflection spectrum. Light reflected from the grating interferes with Fresnel reflected light at the air-substrate interface. This interference pattern is clearly visible in our measurements as shown in Figs. 6(d) and 7(b). For the numerical simulations shown in section 2 the substrate was assumed to be infinite. For accurate comparison with our measurements this finite substrate of thickness 1 mm was included when calculating the numerically predicted reflectivities shown in Figs. 6(c) and 7(a).

While this interference pattern can be predicted it is a concern in terms of grating performance as a sensor. While a re-design of the physical structure of the grating could address this issue, commercial software packages such as unscrambler [36] can be used to mitigate the impact of this interference as shown in Fig. 7(d). In this Fig. the measured data is presented after it has

been filtered within the unscrambler software. This post-processing of the grating measurements can thus be used to overcome the impact on sensor performance by removing the interference pattern.

4. Conclusion

We have investigated the potential of SWGs for use as absorption based sensors. We have shown numerically that gratings can be designed such that their performance can equal or surpass that of an ATR which employs 5 internal reflections. We also numerically demonstrated how absorption based sensing performance can be enhanced by native resonant shifts due to changes in the refractive index of the analyte. These native resonant shifts are well documented for sensing purposes, however it was not desired to measure them directly, rather it was desired to use them to enhance the normalised reflectivity response as shown in Section 2.2. Experimentally, we employed a previously fabricated ES-ZCG for the measurement of a number of analyte solutions, each with a different ethanol concentration. These measurements agreed with numerical predictions in terms of overall shape and magnitude of response. As with numerical simulations, the measured reflectivity response for TM polarised light was in response to the material absorption bands of ethanol and water. Measurements made with TE polarised light demonstrate the use of a resonant wavelength shift owing to interaction with the real part of the refractive index in addition to absorption based sensing to enhance the normalised reflectivity response of the sensing probe. This agreement between experiment and theory as well as our numerical simulations highlights the promise of using these sub-wavelength structures for absorption based sensing, particularly in such an important wavelength range.

That being said, the interference patterns visible in Figs. 6(d) and 7(b) require attention in terms of their impact on the performance of the SWG sensing transducers. With post processing, as shown in Fig. 7(d) this interference pattern can be removed, however there is still an attendant noise signal which would impact the sensing capabilities of the device. When comparing Figs. 7(b) and 7(d) a similar noise profile for pure water solutions is present in both cases, indicating that the noise present is attributable to the light source and detector used in this experiment.

In this work, SWGs are proposed as sensing probes for use as part of a larger sensing system. Currently the ATR is the sensor probe of choice for absorption based sensing in the fingerprint region. Sources and detectors commonly used with the ATR include QCL and Quantum Cascade Detector (QCD) as well as the FTIR. For a realistic comparison with the sensing potential of an ATR sensor, peak to peak signal to noise values (12500:1) [37] for the Agilent Cary 670 FTIR spectrometer when used with an ATR in the 1000 cm^{-1} region was used to calculate a potential limit of detection value of the ES-ZCG sensor used for experimental measurements. Using the filtered measurements from Fig. 7(d) where a 24.24% drop in normalised reflectivity occurs between 0% and 20% ethanol solutions. Using the condition that a sample is detectable if it induces a change which is 3 times greater than the p-p noise a potential limit of detection value of 0.02% ethanol is calculated.

As well as having a superior reflectivity response to absorptive species, SWGs use a single reflection at normal incidence and typically have much smaller footprints than ATR crystals. Operating at normal incidence also allows optical components such as fibres and waveguides to be used with a SWG sensor. Considering the continued appetite for advancement towards integrated photonic sensors, devices such as the gratings described herein should be seen as promising enabler for future absorption based sensing devices.

Funding

Science Foundation Ireland (SFI) (12/RC/2276); Irish Government's Programme for Research in Third Level Institutions, Cycle 5, Strand 1a (CREATE); Cork Institute of Technology (CIT) (RISAM).

Acknowledgments

The authors gratefully acknowledge funding support from Science Foundation Ireland, contract no. 12/RC/2276 (IPIC). Supported by the Irish Government's Programme for Research in Third Level Institutions, Cycle 5, Strand 1a (CREATE). We also gratefully acknowledge support of the RISAM PhD scholarship programme from Cork Institute of Technology.

References

1. M. H. Elshorbagy, A. Cuadrado, and J. Alda, "High-sensitivity integrated devices based on surface plasmon resonance for sensing applications," *Photon. Res.* **5**, 654–661 (2017).
2. R. Li, D. Wu, Y. Liu, L. Yu, Z. Yu, and H. Ye, "Infrared plasmonic refractive index sensor with ultra-high figure of merit based on the optimized all-metal grating," *Nanoscale Res. Lett.* **12**, 1 (2017).
3. J. Langer, S. M. Novikov, and L. M. Liz-Marzan, "Sensing using plasmonic nanostructures and nanoparticles," *Nanotechnology* **26**, 322001 (2015).
4. W. Kong, Z. Zheng, Y. Wan, S. Li, and J. Liu, "High-sensitivity sensing based on intensity-interrogated Bloch surface wave sensors," *Sensors Actuators B: Chem.* **193**, 467–471 (2014).
5. P. Munzert, N. Danz, A. Sinibaldi, and F. Michelotti, "Multilayer coatings for Bloch surface wave optical biosensors," *Surf. Coatings Technol.* **314**, 79–84 (2017).
6. Q. Yang, L. Qin, G. Cao, C. Zhang, and X. Li, "Refractive index sensor based on graphene-coated photonic surface-wave resonance," *Opt. Lett.* **43**, 639–642 (2018).
7. Y. Liu, Y. Li, M. Li, and J.-J. He, "High-sensitivity and wide-range optical sensor based on three cascaded ring resonators," *Opt. Express* **25**, 972–978 (2017).
8. W. Yang, S. Song, X. Yi, S. X. Chew, L. Li, and L. Nguyen, "Silicon-on-insulator microring resonator sensor based on an amplitude comparison sensing function," *Opt. Lett.* **43**, 70–73 (2018).
9. Y. Liu, G. Wu, R. Gao, and S. Qu, "High-quality Mach-Zehnder interferometer based on a microcavity in single-multi-single mode fiber structure for refractive index sensing," *Appl. Opt.* **56**, 847–853 (2017).
10. Q. Wang, B. T. Wang, L. X. Kong, and Y. Zhao, "Comparative analyses of bi-tapered fiber Mach Zehnder interferometer for refractive index sensing," *IEEE Transactions on Instrumentation Meas.* **66**, 2483–2489 (2017).
11. S. S. Wang and R. Magnusson, "Design of waveguide-grating filters with symmetrical line shapes and low sidebands," *Opt. Lett.* **19**, 919–921 (1994).
12. S. S. Wang and R. Magnusson, "Multilayer waveguide-grating filters," *Appl. Opt.* **34**, 2414–2420 (1995).
13. C. F. R. Mateus, M. C. Y. Huang, Y. Deng, A. R. Neureuther, and C. J. Chang-Hasnain, "Ultrabroadband mirror using low-index cladded subwavelength grating," *IEEE Photonics Technol. Lett.* **16**, 518–520 (2004).
14. V. Karagodsky, F. G. Sedgwick, and C. J. Chang-Hasnain, "Theoretical analysis of subwavelength high contrast grating reflectors," *Opt. Express* **18**, 16973–16988 (2010).
15. V. Karagodsky and C. J. Chang-Hasnain, "Physics of near-wavelength high contrast gratings," *Opt. Express* **20**, 10888–10895 (2012).
16. F. Lu, F. G. Sedgwick, V. Karagodsky, C. Chase, and C. J. Chang-Hasnain, "Planar high-numerical-aperture low-loss focusing reflectors and lenses using subwavelength high contrast gratings," *Opt. Express* **18**, 12606–12614 (2010).
17. A. B. Klemm, D. Stellinga, E. R. Martins, L. Lewis, G. Huyet, L. O'Faolain, and T. F. Krauss, "Experimental high numerical aperture focusing with high contrast gratings," *Opt. Lett.* **38**, 3410–3413 (2013).
18. B. Hogan, S. P. Hegarty, L. Lewis, J. Romero-Vivas, T. J. Ochaliski, and G. Huyet, "Realization of high-contrast gratings operating at 10 μm ," *Opt. Lett.* **41**, 5130–5133 (2016).
19. B. Hogan, L. Lewis, J. Romero-Vivas, T. J. Ochaliski, and S. P. Hegarty, "Resonant gratings with an etch-stop layer and a fabrication-error tolerant design," *Opt. Express* **26**, 13205–13213 (2018).
20. Y. Kato, M. Kikugawa, and E. Sudo, "Attenuated Total Reflection Surface-Enhanced Infrared Absorption (ATR SEIRA) spectroscopy for the analysis of fatty acids on silver nanoparticles," *Appl. Spectrosc.* **71**, 2083–2091 (2017).
21. C. Gasser, J. Kilgus, M. Harasek, B. Lendl, and M. Brandstetter, "Enhanced mid-infrared multi-bounce ATR spectroscopy for online detection of hydrogen peroxide using a supercontinuum laser," *Opt. Express* **26**, 12169–12179 (2018).
22. N. J. Harrick, "Electric field strengths at totally reflecting interfaces," *J. Opt. Soc. Am.* **55**, 851–857 (1965).
23. M. G. Moharam, T. K. Gaylord, E. B. Grann, and D. A. Pommet, "Formulation for stable and efficient implementation of the rigorous coupled-wave analysis of binary gratings," *J. Opt. Soc. Am. A* **12**, 1068–1076 (1995).
24. M. G. Moharam, T. K. Gaylord, D. A. Pommet, and E. B. Grann, "Stable implementation of the rigorous coupled-wave analysis for surface-relief gratings: enhanced transmittance matrix approach," *J. Opt. Soc. Am. A* **12**, 1077–1086 (1995).
25. P. Lalanne and G. M. Morris, "Highly improved convergence of the coupled-wave method for TM polarization," *J. Opt. Soc. Am. A* **13**, 779–784 (1996).
26. V. Liu and S. Fan, "S4: A free electromagnetic solver for layered periodic structures," *Comput. Phys. Commun.* **183**, 2233–2244 (2012).
27. S. Adachi, *Optical Constants of Crystalline and Amorphous Semiconductors* (Springer US, 1999).
28. E. Palik, *Handbook of Optical Constants of Solids* (Academic, 1998).

29. J. Kischkat, S. Peters, B. Gruska, M. Semtsiv, M. Chashnikova, M. Klinkmüller, O. Fedosenko, S. Machulik, A. Aleksandrova, G. Monastyrskyi, Y. Flores, and W. T. Masselink, "Mid-infrared optical properties of thin films of aluminum oxide, titanium dioxide, silicon dioxide, aluminum nitride, and silicon nitride," *Appl. Opt.* **51**, 6789–6798 (2012).
30. L. Gao, F. Lemarchand, and M. Lequime, "Exploitation of multiple incidences spectrometric measurements for thin film reverse engineering," *Opt. Express* **20**, 15734–15751 (2012).
31. G. M. Hale and M. R. Querry, "Optical constants of water in the 200-nm to 200- μ m wavelength region," *Appl. Opt.* **12**, 555–563 (1973).
32. E. Sani and A. Dell'Oro, "Spectral optical constants of ethanol and isopropanol from ultraviolet to far infrared," *Opt. Mater.* **60**, 137–141 (2016).
33. A. Liu, W. H. E. Hofmann, and D. H. Bimberg, "Integrated high-contrast-grating optical sensor using guided mode," *IEEE J. Quantum Electron.* **51**, 1–8 (2015).
34. R. Magnusson, D. Wawro, S. Zimmerman, and Y. Ding, "Resonant photonic biosensors with polarization-based multiparametric discrimination in each channel," *Sensors* **11**, 1476–1488 (2011).
35. J. G. Wangüemert-Pérez, P. Cheben, A. Ortega-Moñux, C. Alonso-Ramos, D. Pérez-Galacho, R. Halir, I. Molina-Fernández, D.-X. Xu, and J. H. Schmid, "Evanescent field waveguide sensing with subwavelength grating structures in silicon-on-insulator," *Opt. Lett.* **39**, 4442–4445 (2014).
36. Camo-Software, *Unscrambler X Data analysis software package V10.5*.
37. Agilent Inc, "Highest available signal-to-noise performance, delivering superior sensitivity and analytical performance," <https://www.agilent.com/cs/library/technicaloverviews/public/si-1353.pdf> (11-26-2018).